

# Direct structural observation of a molecular junction by high-energy x-ray reflectometry

Michael Lefenfeld<sup>\*†</sup>, Julian Baumert<sup>†‡</sup>, Eli Sloutskin<sup>§</sup>, Ivan Kuzmenko<sup>¶</sup>, Peter Pershan<sup>||</sup>, Moshe Deutsch<sup>§</sup>, Colin Nuckolls<sup>\*</sup>, and Benjamin M. Ocko<sup>\*\*\*</sup>

<sup>\*</sup>Department of Chemistry, Columbia University, New York, NY 10027; <sup>†</sup>Department of Physics, Brookhaven National Laboratory, Upton, NY 11973; <sup>§</sup>Department of Physics, Bar-Ilan University, Ramat-Gan 52900, Israel; <sup>¶</sup>Complex Materials Consortium Collaborative Access Team (CMC-CAT), Advanced Photon Source, Argonne National Laboratory, Argonne, IL 60439; and <sup>||</sup>Department of Physics, Harvard University, Cambridge, MA 02138

Edited by Stuart Lindsay, Arizona State University, Tempe, AZ, and accepted by the Editorial Board December 12, 2005 (received for review September 9, 2005)

**We report a direct angstrom resolution measurement of the structure of a molecular-size electronic junction comprising a single (or a double) layer of alkyl-thiol and alkyl-silane molecules at the buried interface between solid silicon and liquid mercury. The high-energy synchrotron x-ray measurements reveal densely packed layers comprising roughly interface-normal molecules. The monolayer's thickness is found to be 3–4 Å larger than that of similar layers at the free surfaces of both mercury and silicon. The origins of this and the other unusual features detected are discussed in this article. Measurements of the bilayer junction with an applied potential did not show visible changes in the surface normal structure.**

monolayers | structure | x-ray reflectivity | molecular electronics

In nanoscience and nanotechnology and, in particular, the emerging field of molecular electronics, individual molecules have to be inserted into a nanoscale environment such that they perform a prescribed electronic function. Clearly, the function and performance of the devices depend critically on the structure and packing of the molecules (1). Yet, studying the structure of such devices poses formidable experimental challenges. To make further progress, it is important to systematically study the structural properties of these surfaces and interfaces after molecules have been brought into contact with their supporting electrode. Deeply buried interfaces and nanolayers, in particular, are inaccessible to scanning probe and high-resolution electron microscopy techniques. Hipps *et al.* have used both inelastic electron tunneling spectroscopy (2) and surface Raman spectra (3) to obtain structural information of buried junctions, but without achieving angstrom resolution. Raman and Fourier transform infrared measurements of similar resolution levels also have been carried out (4, 5). We present here an angstrom resolution direct determination of the structure of such buried junctions comprising a single or a double organic molecular layer at the interface between two electrodes: mercury and silicon. This study employs the intense, highly focused, high-energy x-ray beam available at synchrotron sources to penetrate through the silicon electrode to the buried layer, giving the ability to determine their molecular structure.

With an eye on functionality for molecular electronic devices, we have chosen to study films of alkyl-thiols and alkyl-silane monolayers, which are widely investigated for molecular electronics applications because of their intrinsically simple molecular structure, their known epitaxial structure on solid supports, their potential as thin-film insulators, and their strong binding to at least one of the electrodes studied here. The organic film is sandwiched between a solid silicon substrate and a mercury droplet. The liquid mercury surface has many advantages as a substrate for self-assembled monolayers (SAMs), compared to solid supports. It is atomically smooth, absent of steps and pits, and conforms to the shape of contacting surfaces. Lacking, as any liquid, intrinsic long-range structure, it does not impose its

own structure on the monolayer by epitaxy, as does, for example, a crystalline Au (111) substrate on alkyl-thiol monolayers (6, 7). These features, along with its noble chemical character, make the mercury electrode an ideal choice for fundamental studies of charge transfer through SAMs in contact with another Hg electrode (8), a solid metal, or a doped semiconductor electrode (9–11). Although the structure of SAMs has been investigated on the free surface of solid metals (6, 7), insulators (12), liquid mercury (13, 14), and aqueous supports (15) by using a variety of techniques, they have not previously been investigated at buried interfaces.

## Results and Discussion

Fig. 1 shows the x-ray reflectivity of the interface between the Hg surface and the clean Si wafer. The background, measured by rotating the sample slightly away from the specular condition, has been subtracted. The solid line is the Fresnel reflectivity,  $R_F(q_z)$ , of an ideally smooth Si/Hg interface of zero width. It is calculated from the critical wave vector,  $q_c = 0.0605 \text{ \AA}^{-1}$ , obtained from the known bulk electron densities of Si and Hg. This  $q_c$  corresponds to a grazing incidence angle, relative to the surface of the sample, of  $0.106^\circ$  of the x-ray beam at 32 keV. The monotonic decrease of the reflected intensity by over eight orders of magnitude to  $1.2 \times 10^{-8}$  at  $q_z = 0.6 \text{ \AA}^{-1}$  shows that the buried interface is clean and that there is no uniform film of impurities in the junction. The deviation of the measured  $R(q_z)$  from  $R_F(q_z)$  can be accounted for by assuming a 4.4-Å Gaussian roughness for the interface (dashed curve). This roughness is close to that determined for the Si wafer at the air interface before the experiments but exceeds the intrinsic 1-Å capillary roughness of the mercury/vapor interface (14), demonstrating that the roughness of the interface is determined by the silicon substrate.

The measured x-ray reflectivities of the octadecanethiol ( $C_{18}SH$ ), the octadecyltrichlorosilane (OTS), and the bilayer molecular junctions, normalized by the Fresnel reflectivity ( $R/R_F$ ), are shown in Fig. 2. Whereas a single interface leads to a monotonically decreasing reflectivity (Fig. 1), the presence of an organic layer gives rise to interference between x-rays reflected from the organic layer/silicon and the organic layer/mercury interfaces, as shown in Fig. 4. As  $q_z$  is varied, this interference creates an oscillatory modulation of the reflected intensity, a pattern known as Kiessig fringes (13, 14, 16). The absence of fringes in Fig. 1 for the “empty” Si/Hg junction suggests that the

Conflict of interest statement: No conflicts declared.

This paper was submitted directly (Track II) to the PNAS office. S.L. is a guest editor invited by the Editorial Board.

Abbreviations: SAM, self-assembled monolayer; OTS, octadecyltrichlorosilane;  $C_{18}SH$ , octadecanethiol; vdW, van der Waals;  $I-V$ , current-voltage.

<sup>†</sup>M.L. and J.B. contributed equally to this work.

<sup>\*\*</sup>To whom correspondence should be addressed. E-mail: ocko@bnl.gov.

© 2006 by The National Academy of Sciences of the USA

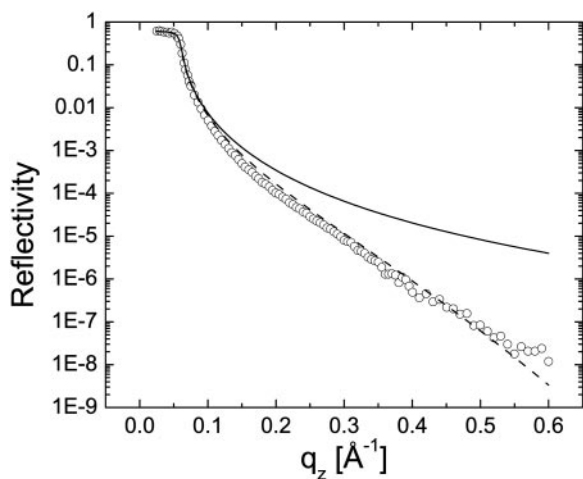


**Fig. 1.** X-ray reflectivity of the Si/Hg interface at room temperature (○) in the absence of an organic SAM. The solid line shows the calculated Fresnel reflectivity,  $R_F$ . The dashed line is the reflectivity expected for the same interface with a 4.4-Å roughness.

Hg is in direct contact with the silicon oxide, and no intermediate organic layer is present. By the same token, the clear Kiessig fringes observed in all reflectivities shown in Fig. 2 manifest the presence of an organic film between the silicon and the mercury. The Kiessig fringe spacing is given by  $\Delta q_z = 2\pi/L$ , where  $L$  is the organic layer thickness. The amplitude of the fringes is related to the electron density in the various regions of the junction. Compared to organic monolayers at the liquid/air interface, the reflectivity modulations are out-of-phase by  $\pi/L$ . This difference arises because at the air interface the electron density increases monotonically, whereas for the present junctions, the electron density change has a different sign at the two interfaces.

In Fig. 2 *a* and *b*, the reflectivity curves of the monolayer junctions of C<sub>18</sub>SH and OTS are shown. Kiessig fringes with periods of  $\Delta q_z \approx 0.21 \text{ \AA}^{-1}$  and  $\Delta q_z \approx 0.23 \text{ \AA}^{-1}$ , corresponding to layer thicknesses of  $\approx 29.9 \text{ \AA}$  and  $\approx 27.3 \text{ \AA}$ , respectively, are clearly evident. In the case of the bilayer junction, Fig. 2*c*, the period of the Kiessig fringes decreases significantly to  $\Delta q_z \approx 0.13 \text{ \AA}^{-1}$ , yielding a total film thickness of  $\approx 52.4 \text{ \AA}$ . At the Hg/air interface, the C<sub>18</sub>SH SAM is known to display a thickness of 25.2 Å (14), whereas at the Si/air interface, the OTS SAM has a thickness of 24.2 Å (17). Both of these values are smaller than the respective thicknesses determined for the corresponding buried monolayers. The thickness of the buried bilayer is also found to be larger than the sum of the monolayer thicknesses at the air interface (49.4 Å). However, it is considerably smaller than the sum of the thicknesses of the two monolayer junctions (57.2 Å).

The reflectivities were analyzed additionally by using the Parratt formalism (18) to obtain the electron density profile of the junction from the measured reflectivity. Although the electron density profile of the C<sub>18</sub>SH buried interface could be modeled by a simple “box model” with a uniform density for each box, this was not possible for the other two molecular junctions. A model-free approach was used for these two junctions. Here an initial density profile is first chosen. It is then divided into a large number of thin (2.0-Å) layers, the densities of which are varied iteratively until a minimum  $\chi^2$  value is reached. For our SAMs, a uniform-density layer was chosen as the starting profile. Its thickness was determined from the period of the Kiessig fringes observed in the measured reflectivity curve. The resulting fits (solid lines) and the corresponding electron densities (*Insets*) are displayed in Fig. 2.

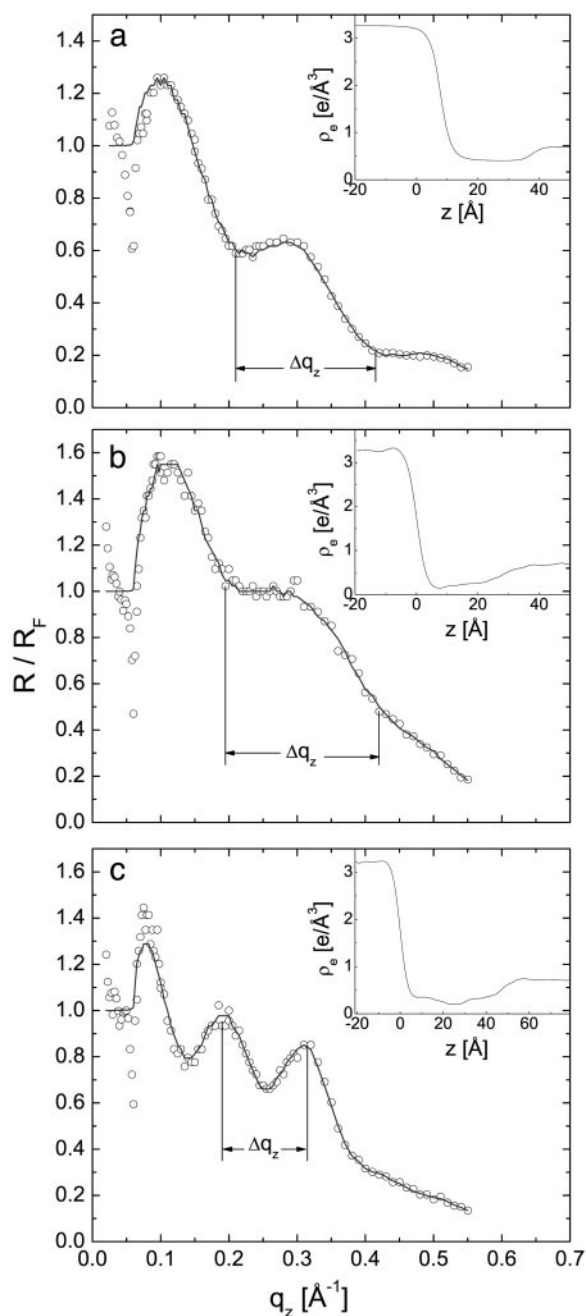


**Fig. 2.** Fresnel-normalized, room-temperature measured reflectivities (○) and model fits (solid lines) of the Si-C<sub>18</sub>SH-Hg (*a*), Si-OTS-Hg (*b*), and Si-OTS-C<sub>18</sub>SH-Hg (*c*) buried junctions. The error bars are smaller than the data symbols. *Insets* show the electron density profiles derived from the corresponding model fits.

For the Si-thiol-Hg interface, a good fit was obtained by using the box model with two independent layers: the first layer models the mercury surface layer, and the second layer models the C<sub>18</sub>SH monolayer bonded to the Hg. The mercury surface layer is found to display a more gradual density decay at the monolayer/mercury interface than that of a clean mercury/air interface (19, 20). This decay might result from the lower density of the bonded sulfur compared to the mercury. The fit yields a monolayer thickness of  $29.6 \pm 0.4 \text{ \AA}$ , consistent with the Kiessig fringe analysis, an electron density of  $0.40 \text{ e/\AA}^3$ , and a roughness of  $3.0 \text{ \AA}$  at the silicon interface. The electron density of the



out to ensure electrical contact and the absence of shorts. Although our results for this single junction are in general agreement with the expected exponential-like  $I$ - $V$  characteristics (10, 11), some variability is observed among the several individual junctions measured. Thus, further measurements are required before a reliable  $I$ - $V$  curve can be presented for this junction.

The constant intensity in Fig. 3 clearly indicates that there is no detectable structural change despite a three-order-of-magnitude change in the current density. The reflectivity scans at several voltages also showed no detectable changes. Together, these results show that the compression of the junction is  $<2\%$  for applied electric potentials in the range of  $\pm 1$  V. We note that the potential drop across the organic junction is somewhat reduced by the potential drop across the low-resistance native oxide. The contraction expected in the junction spacing can be estimated from the pressure induced by the voltage applied across the molecular junction. The pressure across the junction is given by  $P = \epsilon \epsilon_0 V^2 / 2d^2$ , where  $\epsilon = 2.2$  is the dielectric constant of alkane thiols (1) and  $\epsilon_0 = 8.854 \times 10^{-12}$  F/m is the permittivity of free space. For a gap of  $d = 5 \times 10^{-9}$  m and  $V = 1.0$  V, the calculated pressure is  $\approx 4$  bars (1 bar = 100 kPa). By using the bulk compressibility of dodecane (99 ppm/bar) (21), the expected change in the gap spacing is  $\approx 0.04\%$ . This very small change in the gap spacing is consistent with the voltage independence of the reflectivity. Thus, these results suggest that the  $I$ - $V$  curves for this junction should not be dominated by structural changes associated with electrostatically induced compression.

In conclusion, this article demonstrates that x-ray reflectivity can be used to study in detail deeply buried self-assembled molecular layers. The method employs high-energy x-ray beams and allows determination of the molecular structure and phase with angstrom resolution, providing the first evidence of densely packed SAMs in buried interfaces. This method also has the capability of examining a range of molecules on two very important substrates at different surface coverages. The x-ray reflectivity measurements of the molecular junctions formed by either silane or thiol chemistry further illustrate the versatility of this technique. The combination of silane and thiol monolayers to a bilayer within the junction demonstrates the sensitivity of the experimental method toward structural changes within the buried interface. Measurements of the bilayer junction with an applied potential did not show visible changes in the surface normal structure. Because the compression scales as the square of the voltage-to-thickness ratio, junctions with shorter molecules and higher voltages should show noticeable structural changes. For example, a junction with a 1-nm gap at 2 V gives an estimated 4% change in the junction thickness, which should be observable as a change in the period of the Kiessig fringes in the x-ray reflectivity. Overall, combining x-ray reflectivity measurements with  $I$ - $V$  measurements should help to provide a better understanding of the structure-function relationship in a variety of molecular junctions.

## Materials and Methods

Fig. 4 illustrates the experimental x-ray reflectivity geometry (16). This technique measures the Fourier transform of the laterally averaged electron density distribution in the surface normal direction. For a direct observation of the molecular structure of the buried interface, penetrating, high-energy x-ray beams are necessary (22). We have used beamline X-22A at the National Synchrotron Light Source of the Brookhaven National Laboratory, with an energy of 32 keV and a beam cross section of  $0.1 \times 0.5$  mm<sup>2</sup>. Additional measurements were carried out at ID9 with an energy of 24 keV at the Advanced Photon Source of the Argonne National Laboratory. At 32 keV, the beam passes through the 5-mm length of the silicon electrode ( $5 \times 5 \times 1$

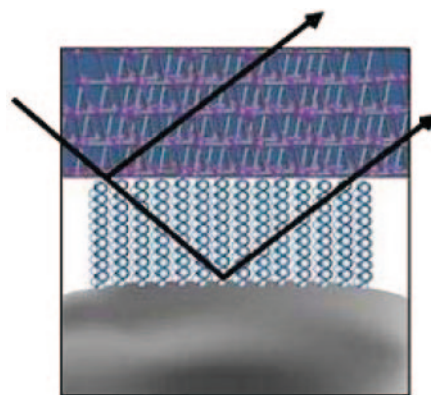


**Fig. 4.** A schematic of the deeply buried monolayer of  $C_{18}$  chains, residing between the upper silicon electrode and lower mercury electrode. The entry and exit of the probing x-ray beam through the top silicon electrode is also shown.

mm<sup>3</sup>), which is comparable to the 4-mm x-ray attenuation length and is reflected from the Si-organic molecule-Hg junction exiting from the other side of the silicon electrode. The reflectivity  $R(q_z)$  is the fraction of the incident intensity reflected by the interface, measured as a function of the wave vector transfer  $q_z$ , and corrected for the illuminated area.

Silicon wafers, (100) orientation, covered with their native oxide, supplied by Umicore Semiconductor Processing (Boston) and cut to the appropriate dimensions, were used as substrates. The wafers are cleaned in a sulfuric acid:hydrogen peroxide ( $H_2SO_4:H_2O_2$ ; 70:30) mixture and rinsed in ultra-pure water before the experiments. Two methods were used to prepare the buried junctions. The first approach used  $C_{18}SH$  covalently bonded to the Hg surface at high coverage. In this Langmuir film approach, the  $C_{18}SH$  is dissolved in chloroform to create a micromolar solution, which is deposited on the free Hg surface (14). After the chloroform evaporates, an alkyl-thiol monolayer is formed. The area per molecule is calculated from the Hg surface area of  $\approx 150$  mm<sup>2</sup>, calculated from the diameter of the circular Kel-F trough containing the mercury and the number of deposited molecules. The molecular surface coverage was chosen to be  $\approx 19$  Å<sup>2</sup> per molecule, corresponding to a closely packed monolayer of fully extended, surface-normal aligned hydrocarbon chains (14). Next, the silicon wafer is lowered by a micrometer onto the mercury, which is contained in a Kel-F trough within a clean, sealed, aluminum sample cell. Once contact is made with the Hg surface, the wafer is raised until a slight capillary rise of the Hg surface is observed through visual inspection. This procedure ensures that the mercury does not block the entrance or exit of the x-ray beam through the side of the Si wafer. The second approach to making molecular junctions uses a SAM of OTS, also an 18 carbon methyl-terminated molecule. Here, the OTS molecules are chemically bound to the native silicon oxide during extended immersion in either bicyclohexyl (ref. 23 and references therein) or toluene (24) solutions containing OTS. The contact between the OTS-covered silicon and the clean Hg surface was made by using the same procedure. A bilayer can also be formed by bringing the OTS-covered silicon into contact with the  $C_{18}SH$ -coated mercury. When applying an electric potential to the molecular junction, the native oxide on the back of the Si wafer is scratched, and conductive silver paint is applied to ensure good electric contact to the wafer. Because we did not visually observe a dewetting of the interface by the mercury or a rise of the mercury onto the sides of the wafer after the potential was applied, we excluded the possibility that the area of the junction changed. The x-ray reflectivity measurements were then performed at room temperature.

M.L. and C.N. acknowledge financial support from the Nanoscale Science and Engineering Initiative of the National Science Foundation under National Science Foundation Award Number CHE-0117752 and from the New York State Office of Science, Technology, and Academic Research. Work at Brookhaven National Laboratory is supported by the

U.S. Department of Energy, Division of Materials Science, under Contract DE-AC02-98CH10886. Support to M.D. by the German-Israeli Foundation, Jerusalem (GIF), is gratefully acknowledged. P.P. acknowledges support from the National Science Foundation under Grant NIRT 03-03916.

1. Slowinski, K., Chamberlain, R. V., Bilewicz, R. & Majda, M. (1996) *J. Am. Chem. Soc.* **118**, 4709–4710.
2. Hipps, K. W. & Mazur, U. (2002) *Inelastic Electron Tunneling Spectroscopy* (Wiley, Chichester, U.K.).
3. Hipps, K. W., Dowdy, J. & Hoagland, J. J. (1991) *Langmuir* **7**, 5–7.
4. Nowak, A. M., McCreery, R. L. (2004) *J. Am. Chem. Soc.* **126**, 16621–16631.
5. Jun, Y. & Zhu, X.-Y. (2004) *J. Am. Chem. Soc.* **126**, 13224–13225.
6. Poirier, G. E. (1999) *Langmuir* **15**, 1167–1175.
7. Fenter, P., Eberhardt, A. & Eisenberger, P. (1994) *Science* **266**, 1216–1218.
8. Slowinski, K., Fong, H. K. Y. & Majda, M. (1999) *J. Am. Chem. Soc.* **121**, 7257–7261.
9. Rampi, M. A. & Whitesides, G. M. (2002) *Chem. Phys.* **281**, 373–391.
10. Selzer, Y., Salomon, A. & Cahen, D. (2002) *J. Phys. Chem. B.* **106**, 10432–10439.
11. Liu, Y.-J. & Yu, H.-Z. J. (2003) *Chem. Phys. Chem.* **4**, 335–342.
12. Tulevski, G. S., Miao, Q., Fukuto, M., Abram, R., Ocko, B. M., Pindak, R., Steigerwald, M., Kagan, C. & Nuckolls, C. (2004) *J. Am. Chem. Soc.* **126**, 15048–15050.
13. Kraack, H., Ocko, B. M., Pershan, P. S., Sloutskin, E. & Deutsch M. (2002) *Science* **298**, 1404–1407.
14. Ocko, B. M., Kraack, H., Pershan, P. S., Sloutskin, E., Tamam, L. & Deutsch, M. (2005) *Phys. Rev. Lett.* **94**, 017802.
15. Kaganer, V. M., Möhwald, H. & Dutta, P. (1999) *Rev. Mod. Phys.* **71**, 779–819.
16. Als-Nielsen, J. & McMorrow, D. (2001) *Elements of Modern X-Ray Physics* (Wiley, New York).
17. Tidswell, I. M., Ocko, B. M., Pershan, P. S., Wasserman, S. R., Whitesides, G. M. & Axe, J. D. (1990) *Phys. Rev. B.* **41**, 1111–1128.
18. Parratt, L. G. (1954) *Phys. Rev.* **95**, 359–369.
19. Magnussen, O. M., Ocko, B. M., Regan, M. J., Penanen, K., Pershan, P. S. & Deutsch, M. (1995) *Phys. Rev. Lett.* **74**, 4444–4447.
20. DiMasi, E., Tostmann, H., Ocko, B. M., Pershan, P. S. & Deutsch, M. (1998) *Phys. Rev. B.* **58**, R13419–R13422.
21. Cutler, W. G., McMickle, R. H., Webb, W. & Schiessler, R. W. (1958) *J. Chem. Phys.* **29**, 727–740.
22. Reichert, H., Honkimaki, V., Snigirev, A., Engemann, S. & Dosch, H. (2003) *Physica B* **336**, 46–55.
23. Maoz, R., Cohen, S. & Sagiv, J. (1999) *Adv. Mater.* **11**, 55–61.
24. Brzoska, J. B., Shahidzadeh, N. & Rondelez, F. (1992) *Nature* **360**, 719–721.